SEMARAK ILMU PUBLISHING

Journal of Advanced Research in Fluid Mechanics and Thermal Sciences

Journal homepage:
https://semarakilmu.com.my/journals/index.php/fluid_mechanics_thermal_sciences/index
ISSN: 2289-7879

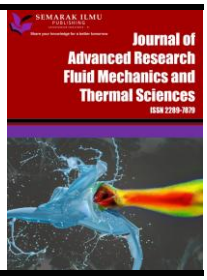

Experimental Study of a Bi-Directional Axial Impulse Turbine for Thermoacoustic Wave Conditions

Wong Choe Tae[1], Fatimah Al Zahrah Mohd Saat[1,2,*], Safarudin Ghazali Herawan[3]

[1] Fakulti Teknologi dan Kejuruteraan Mekanikal (FTKM), Universiti Teknikal Malaysia Melaka (UTeM), Hang Tuah Jaya, 76100 Durian Tunggal Melaka, Malaysia
[2] Green and Efficient Energy Technology (GrEET), Centre for Advanced Research on Energy (CARe), Universiti Teknikal Malaysia Melaka, Hang Tuah Jaya 76100 Durian Tunggal, Melaka, Malaysia
[3] Industrial Engineering Department, Faculty of Engineering, Bina Nusantara University, Jakarta, 11480, Indonesia

ARTICLE INFO

Article history:
Received 26 December 2024
Received in revised form 29 March 2025
Accepted 10 April 2025
Available online 30 April 2025

Keywords:
Bi-directional turbine; thermoacoustics open-closed resonator; 3D print; elliptic nose cone

ABSTRACT

This paper reports a study on optimizing a 3D printed bi-directional axial impulse turbines for thermoacoustic environment with different opening sizes at one end of the resonator. The laboratory tests used a loudspeaker to induce acoustic flow variations. Experiments were conducted to test different variables: the end plate's opening diameter and the use of an elliptic nose cone. Key findings include the optimal 93 mm opening for the maximum voltage and speed of the turbine, the slight improvement in flow dynamics due to the use of the elliptic nose cone, and the identification of the system's resonance frequency at 85 Hz. This study provides insights into the use of the bi-directional axial impulse turbines in thermoacoustic wave conditions for different opening size at one end of the resonator with and without the assistance of guiding cone for the turbine, filling a critical gap in literature and contributing to optimizing thermoacoustic systems for enhanced energy conversion. The results emphasize the importance of tailoring components to optimal frequencies to obtain better efficiency.

1. Introduction

Thermoacoustics is a subfield of thermofluids that uses thermodynamic, acoustic, and fluid mechanics concepts to study the interaction of heat and sound waves in a fluid or gas medium [1]. It studies how temperature variations may generate sound waves and vice versa. Thermal gradients create sound waves in thermoacoustic devices, eliminating the need for mechanical or electrical inputs [2].

Thermoacoustics has gained attention in recent years due to its benefits in comparison to alternative refrigeration and engine systems [3,4]. The utilisation of thermoacoustic technology exhibits the potential to surpass conventional refrigeration techniques in terms of efficiency and environmental sustainability [5]. The latter relies on refrigerant gases that have been identified as

* *Corresponding author.*
E-mail address: fatimah@utem.edu.my

https://doi.org/10.37934/arfmts.130.2.7489

contributors to ozone depletion and global warming [6,7]. The existing literature on thermoacoustic electrical generators (TAEGs) has primarily documented acoustic-to-electric converters such as linear generators, magnetohydrodynamic generators (MHD), piezoelectric transducers, and crank-rod transducers [4]. Additional acoustic-to-electric converters have been identified such as bidirectional turbines and triboelectric nanogenerators [2]. Currently, linear alternators exhibit superior electrical power output and efficiency [8]. While bidirectional turbines (BDT) are not as commonly discussed as linear alternators, recent studies have demonstrated that they exhibited comparable performance metrics and warrant further investigation in future research [2,9].

Bi-directional turbines (BDTs) are capable of converting linear oscillating flow motion, also known as a bi-directional flow, into unidirectional rotational flow motion, making them a notable type of turbine [10,11]. BDTs differ from conventional turbines by eliminating the zero-velocity point, thereby enabling uninterrupted rotation and effective energy conversion [9]. BDTs have potential in thermoacoustic power generation, in addition to their current use in harnessing marine wave energy through Oscillating Water Column (OWC) applications [2].

Thermoacoustic power generation is the process of converting sound waves into work, which can subsequently be transformed into electrical energy. BDTs provide multiple benefits in this context. Their low acoustic impedance enables efficient coupling with high-intensity sound waves [12]. Their mechanical resonance frequency is not affected by the engine's operating frequency, which makes them versatile [13]. BDTs can be manufactured inexpensively using advanced techniques such as 3D printing. BDTs are a desirable choice for thermoacoustic systems due to their feature of low cooling requirements and the use of inexpensive magnets [9].

The Wells turbine is the fundamental type of BDT utilised in OWC applications [2]. Wells turbines are commonly employed for the conversion of wave energy to electrical energy [14]. Nevertheless, these devices exhibit constraints including restricted flow coefficient range, high-speed operation, and inadequate starting characteristics. To overcome these constraints, Wells turbines have undergone several modifications, including the integration of stationary guide vanes to transform them into impulse turbines [14]. Impulse turbines exhibit superior efficiency at lower starting and operating speeds in comparison to Wells turbines. However, their performance may be inferior to that of the self-pitching impulse turbines [9].

BDTs hold promise as a viable and scalable option for transforming acoustic power into electrical energy in the field of thermoacoustic power generation [15]. The elevated mean pressures and the increased gas density in thermoacoustic engines can enhance turbine efficiency [16]. However, most experimental and computational studies on BDTs under OWC conditions are not directly applicable to thermoacoustic applications due to the differences in system characteristics. Thermoacoustic engines necessitate specific design considerations due to their operation at elevated frequencies and pressures [2].

BDTs can be classified into two primary configurations which are axial impulse turbines and radial impulse turbines [2]. Axial impulse turbines exhibit broad operational capabilities, effective efficiency, and favourable starting attributes [17]. They have widespread applications in diverse fields such as aircraft engines and power generation systems [15]. Radial impulse turbines have lower axial thrust, which can decrease fatigue on generator bearings [9]. The main difference between a bi-directional axial impulse turbine and a bi-directional radial impulse turbine can be observed through the direction of the fluid flow and the arrangement of the turbine blades. The axial turbine has blades arranged parallel to the shaft while the radial turbine has blades arranged radially outward [18]. These differences make each turbine suitable for specific applications based on the characteristics of the fluid flow. BDTs have potential advantages in thermoacoustic power generation due to their cost-effectiveness, compatibility with readily available generators, and suitability for industrial scale-up

[19]. BDTs have potential for sustainable electricity generation through acoustic energy harnessing with additional research and optimisation [2].

The utilisation of bi-directional turbines in conjunction with rotary motors presents a viable substitute in situations that necessitate substantial power output while maintaining cost-effectiveness. Wave energy converters are frequently utilised in oscillating water column (OWC) facilities [9]. The axial-flow impulse bi-directional turbine is a commonly employed technology in oscillating water column (OWC) facilities owing to its extensive operational flow capacity. The bi-directional turbine is comprised of a rotor featuring a symmetric blade configuration, which is encompassed by two sets of guide vanes [9]. The blade's rotation is propelled in a unidirectional manner by the flow originating from either side. Although the design of turbines has been extensively studied in the context of oscillating water columns (OWC), their implementation for the purpose of acoustic power conversion in thermoacoustic engines is a relatively nascent field, primarily due to the distinct working conditions involved [4].

The experimental and numerical investigations that have been conducted on BDTs in the context of oscillating water column (OWC) conditions are not directly transferable to thermoacoustic applications. The reason for this disparity is that the former experiments involved water while thermoacoustic systems are usually operated with gaseous as the working fluid. In addition to that OWC were conducted on unsealed systems, thereby exposing the turbine to the surrounding atmosphere. Conversely, thermoacoustic applications typically employ enclosed systems that may be either pressurised or unpressurized [12]. Furthermore, it has been observed that the frequency of the wave in oscillating water columns (OWCs) is significantly lower than the rotational frequency of bidirectional turbines [18]. However, in the context of thermoacoustic applications, these frequencies may be comparable [9]. Additionally, the numerical investigations documented in OWC were conducted using a quasi-steady approach, given that the frequency of the wave is significantly lower than the angular velocity of the turbine [20]. The assumption is deemed unsuitable for thermoacoustic applications wherein the frequency and turbine angular velocity exhibit comparable magnitudes [2]. In summary, it is imperative to carry out empirical investigations to examine the factors that impact the state of thermoacoustic waves in a bi-directional axial impulse turbine.

While bi-directional axial impulse turbines have shown promise in thermoacoustic energy conversion, there is limited experimental data available regarding the behaviour of bi-directional axial impulse turbines under various thermoacoustic wave conditions [9]. The interaction between unsteady heat release and acoustic disturbances can lead to self-sustained thermoacoustic oscillations and these oscillations are the backbone for the operation of many thermoacoustic prime movers or cooling systems [21]. Thermoacoustic system can be built with either open-open, closed-open or closed-closed resonator ends condition and the fluid dynamics studies for all these conditions, particularly with the involvement of bi-directional turbines, are scarcely reported [22]. Understanding the thermoacoustic wave conditions is essential for designing and optimizing thermoacoustic systems for safe and efficient operation [23]. For a better operation, the use of a cone was suggested to guide the wave into the rotor, particularly in the region near the velocity node where velocity amplitude is weaker [9]. There is a recent work on a smaller-scale version bi-directional turbine with limited capabilities of thermoacoustic energy conversion presumably due to the lower volume of flow at that size [24]. Therefore, this paper is focussing on analysing the wave conditions of thermoacoustics using a larger diameter of bi-directional axial impulse turbine operated in a resonator with different opening size.

2. The 3D Printed Bi-Directional Turbine and Elliptic Nose Cone

In preparation for the experiment, both the bi-directional axial impulse turbine and the elliptic nose cone are designed and manufactured using a 3D printer, specifically the Creality CR-5 Pro model. The bi-directional turbine comprises an upstream stator, a middle rotor, and a downstream stator. To ensure optimal performance, a hub-to-tip ratio of 0.7 is employed, as suggested by the literature [9]. Table 1 provides detail specifications for the designed bi-directional turbine, including parameters such as hub radius, tip radius, blade angle, and the number of blades. All the design parameters, aside from the hub radius and the tip radius, adhere to the recommendations outlined in the published work. Figure 1 shows the bi-directional axial impulse turbine that was designed using SolidWorks while Figure 2 showcases the 3D-printed turbine.

Table 1
Specifications of the bi-directional axial impulse turbine

Parameter	Value
Number of rotor blades	29
Number of guide vanes	26
Blade angle	60°
Mean turbine radius	39.525 mm
Hub radius	32.55 mm
Tip radius	46.5 mm
Hub-to-tip ratio	0.7
Tip clearance	1 mm
Axial spacing (guide vanes to rotor)	1 mm

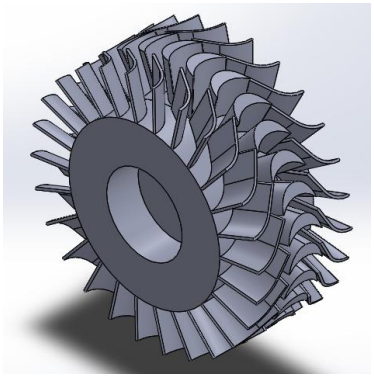

Fig. 1. CAD drawing of the bi-directional turbine

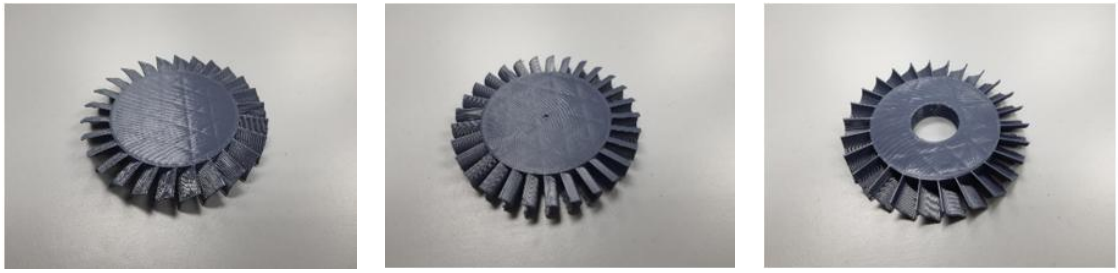

(a) (b) (c)

Fig. 2. The 3D printed (a) upstream stator, (b) middle rotor, and (c) downstream stator

In addition to the bi-directional turbine, the introduction of an elliptic nose cone to the configuration represents another parameter under investigation of the current experiment. Similar to the turbine, the elliptic nose cone is designed and fabricated using 3D printing technology. The shape and dimensions of the nose cone are determined to minimize air resistance and encourage smooth airflow within the experimental setup, as detailed in Table 2. Notably, the diameter of the elliptic nose cone aligns with the hub diameter of the turbine. Figure 3 presents a detailed CAD drawing of the elliptic nose cone while Figure 4 shows a 3D-printed elliptic nose cone.

Table 2
Specifications of elliptic nose cone

Parameter	Dimension (mm)
Length	70
Major axis length	40
Minor axis length	30
Nose cone diameter	65.1
Thickness	2

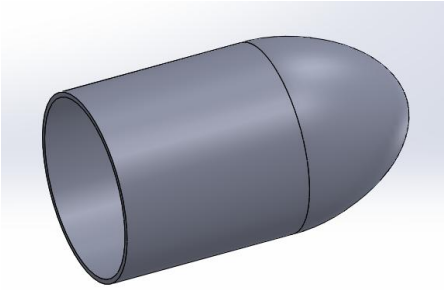

Fig. 3. A CAD drawing of elliptic nose cone

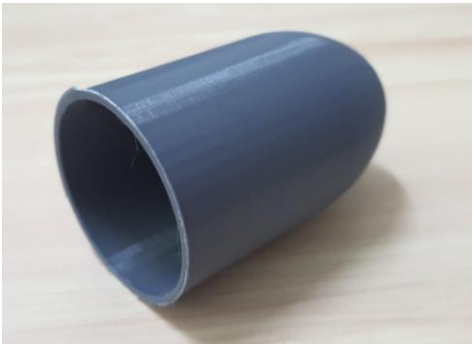

Fig. 4. The 3D printed elliptic nose cone

3. Experimental Setup

The experimental setup shown in Figure 5 illustrates the arrangement and configuration of the experimental apparatus. This setup is designed to provide a controlled and reliable experiment environment for conducting precise measurements and acquiring meaningful data. The function generator is connected to the amplifier, and subsequently linked to the loudspeaker. Specifically, the loudspeaker model utilized is the Mohawk MM-Series MM-6. The function generator model employed in this project is the RS PRO AFG-21005 5 MHz arbitrary function generator, chosen for its capability to generate precise frequency signals. Additionally, the amplifier utilized is the Behringer KM750 Amplifier model. This amplifier is selected for its ability to amplify the output signals from the

function generator effectively, ensuring that the signals transmitted to the loudspeaker are of sufficient amplitude for the experiment's requirements. The loudspeaker is attached to a 183 mm long resonator tube with inner diameter of 93 mm. The bi-directional turbine is assembled at a location near the open end of the resonator. A 12 V motor is securely connected to the bi-directional turbine and fixed within the resonator to facilitate efficient rotation, as depicted in Figure 6. This configuration ensures that the turbine can effectively harness the thermoacoustic flow within the system. To monitor the performance of the system, the wires of the motor are connected to a multimeter, enabling the measurement of the voltage generated during operation. Furthermore, a tachometer is employed to measure the rotational speed of the turbine accurately.

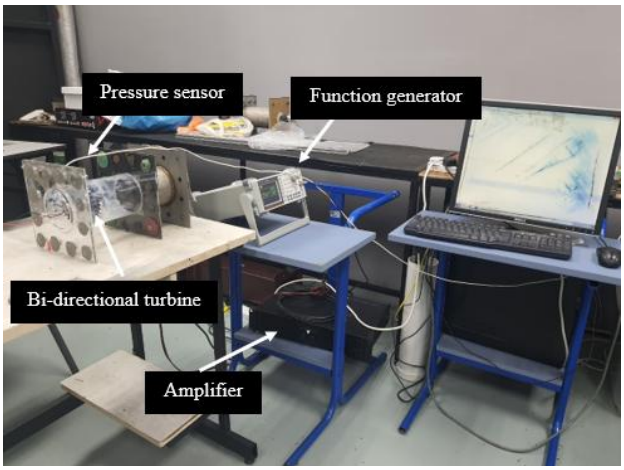

Fig. 5. Experimental setup

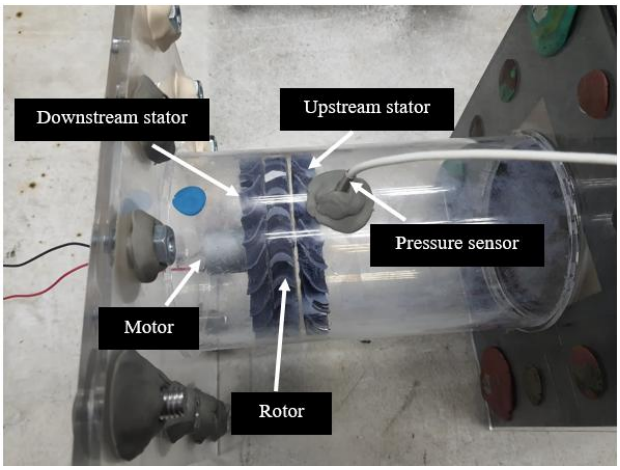

Fig. 6. Close up diagram of the experimental setup

Initially, the experiment focuses on assessing the impact of varying hole diameters that represent the size of opening at the end plate of the resonator. Specifically, hole with diameters of 40 mm, 60 mm, 80 mm, and 93 mm are evaluated. Figure 7 shows the 40 mm diameter of holes at the end of resonator. Subsequently, the integration of an elliptic nose cone into the system is conducted to evaluate its performance, as depicted in Figure 8. Before initiating the experiments, it is important to ensure a secure placement of the resonator, guaranteeing an effective seal to prevent any potential air leakage particularly near the driver’s location.

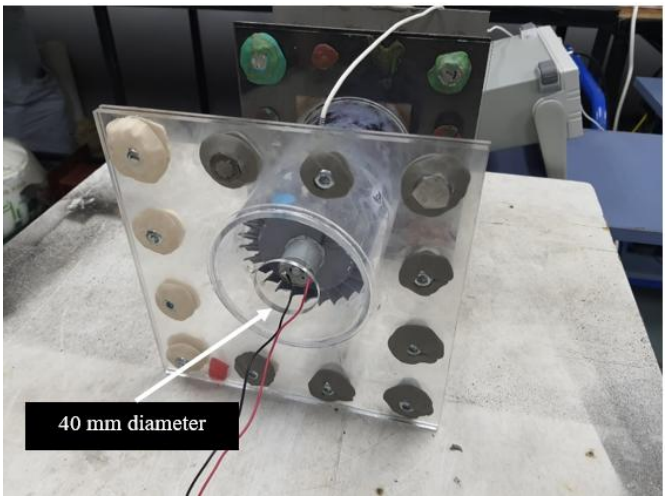

Fig. 7. 40 mm diameter of holes at the end of resonator

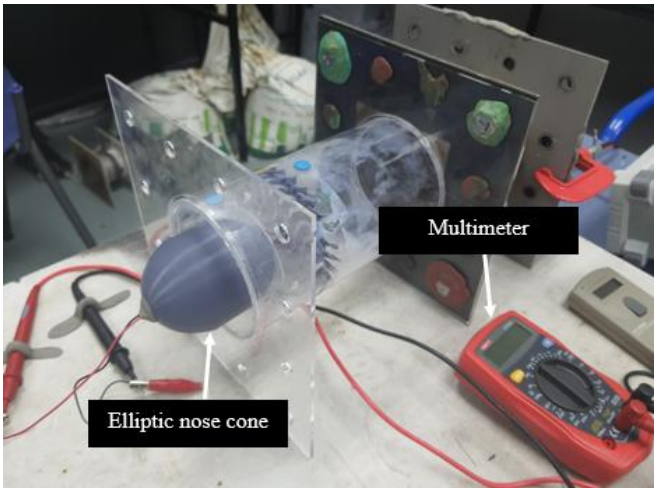

Fig. 8. Elliptic nose cone installation to the system

4. Results and Discussions

Once the data collection phase is completed, the results are carefully analyzed to identify trends, patterns, and correlations. This analysis involves comparing the measurements obtained under different experimental conditions, such as varying hole diameters and the introduction of the elliptic nose cone.

4.1 Impact of Different Diameters of Opening at the End Plate

Thermoacoustic system can be found operating in conditions with open-open, closed-open and closed-closed ends of resonator [22]. Hence the operation of the bi-directional turbine is tested with different opening sizes at one end of the resonator near the pressure antinode. Table 3 shows four different cases with their respective diameters of hole on the end plate to explore the influence of varying diameters on the measured parameters, including angular speed and voltage. Case 4 represents the completely open end with opening diameter similar to the inner diameter of the resonator in the experiment as no acrylic board is placed at the end of resonator. Therefore, diameter of Case 4 will be equalled to the inner diameter of the resonator tube, which is 93 mm.

Table 3
Diameter of the opening at the end plate for each case

Case	Diameters of opening at the end plate (mm)
1	40
2	60
3	80
4	93

With a consistent supplied flow frequency of 65 Hz, the amplitude of the peak-to-peak voltage, Vpp, for the loudspeaker is adjusted, ranging from 0.3 Vpp to 0.5 Vpp, with incremental data points of 0.05 Vpp. The relationship between mean voltage output and the amplitude of the Vpp input is depicted in Figure 9, highlighting variations across different cases.

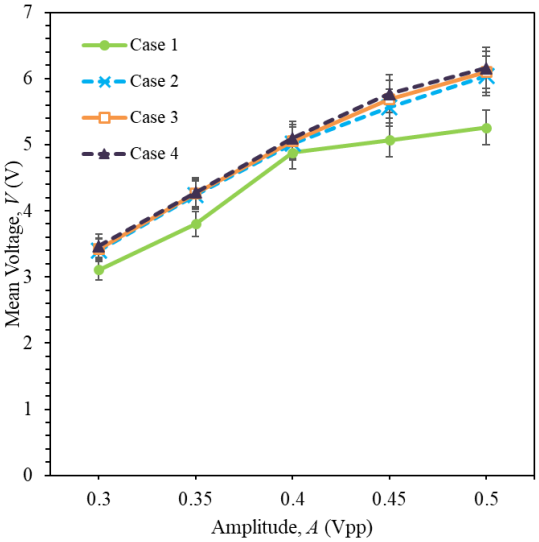

Fig. 9. Mean voltage output from the turbine versus amplitude of peak-to-peak voltage input at constant frequency for different cases

When comparing Case 4, characterized by 93 mm hole diameter, with other cases, it is observed that Case 4 exhibits the highest voltage output, which is 6.16 V at 0.5 Vpp. This phenomenon can be attributed to several factors related to the diameter of the hole at the end of resonator. Firstly, the bigger hole diameter reduces the impedance encountered by the acoustic waves within the system. This reduction in impedance allows for a more efficient transfer of energy within the system, leading to higher voltage output. The acoustic waves encounter less reflection and interference, promoting a smoother flow and transfer of thermoacoustic energy [25].

Apart from that, it can be observed that as amplitude of the system increases, the voltage for all the cases increases as well. When the amplitude increases, it means that the particles are undergoing larger oscillations. In a thermoacoustic system, this mechanical displacement can be directly related to the generation of electrical voltage [25]. This is because larger amplitude corresponds to more significant pressure variations in the medium. This increased pressure, in turn, causes larger displacements of particles in the medium. These dynamic pressure variations promote greater deformation and, consequently, a higher voltage output. Besides, the mechanical displacement of particles is not only a consequence of the acoustic waves but is intricately linked to the transfer of energy within the system. As the amplitude increases, more energy is imparted to the medium. This energy is then translated into larger mechanical displacements, especially in regions where the

system is designed to convert these displacements into electrical energy. The consistency between these results reinforces the significance of maintaining a specific amplitude level, highlighting its direct impact on the efficiency and effectiveness of the bi-directional turbine in converting acoustic energy into mechanical work [26].

Moreover, it can be noticed that the difference between the mean voltages obtained for various cases progressively diminishes. The widest gap is observed between Case 1 and Case 2, whereas the smallest disparity is noted between Case 3 and Case 4. The narrowing gap between the mean voltages for the different cases signifies a trend of converging performance as the end cover diameters vary. The notable distinction in performance between Case 1 and Case 2 suggests that smaller end cover diameters tend to exhibit more prominent differences in voltage generation. As the end cover diameter increases from Case 2 to Case 4, the observed trend implies a diminishing impact of diameter variation on voltage output. This could be attributed to the fact that, at 93 mm diameter which equals to the diameter of resonator, the system reaches a state of relative equilibrium where further increments in diameter of hole do not substantially affect performance.

In addition to voltage, another measured parameter is angular speed of the rotor of bi-directional turbine. The mean angular speed of rotor for the different cases is shown in Figure 10. From the graph, it is clearly shown that the angular speed of rotor for every case increases as the amplitude increases. Comparing four of the cases, the highest angular speed is found to be at Case 4 with 93 mm hole at the end plate. The subsequent cases, characterized by decrease hole diameters, reveal a gradual decline in rotor speed. Specifically, Case 1, featuring a 40 mm hole diameter, exhibits the lowest angular speed. This observed trend aligns with the inherent dynamics of the system, where alterations in the hole diameter introduce distinct impedance effects, influencing the mechanical responses of the turbine [2]. A smaller hole diameter creates a more confined space for the flow of the working medium. This leads to increased aerodynamic resistance against the rotor blades as they try to push through the constrained space, thereby slowing down the rotor. Besides, the smaller diameter hole on the end plate introduces more disturbances in the flow of the working medium. These disturbances can cause turbulence and uneven pressure distribution around the rotor, contributing to a decrease in rotational speed.

From the graph, it is clearly shown that the angular speed of rotor for every case increases as the amplitude increases. Comparing four of the cases, the highest angular speed is found to be at Case 4 with 93 mm hole at the end plate. The subsequent cases, characterized by decrease hole diameters, reveal a gradual decline in rotor speed. Specifically, Case 1, featuring a 40 mm hole diameter, exhibits the lowest angular speed. This observed trend aligns with the inherent dynamics of the system, where alterations in the hole diameter introduce distinct impedance effects, influencing the mechanical responses of the turbine [2]. A smaller hole diameter creates a more confined space for the flow of the working medium. This leads to increased aerodynamic resistance against the rotor blades as they try to push through the constrained space, thereby slowing down the rotor. Besides, the smaller diameter hole on the end plate introduces more disturbances in the flow of the working medium. These disturbances can cause turbulence and uneven pressure distribution around the rotor, contributing to a decrease in rotational speed.

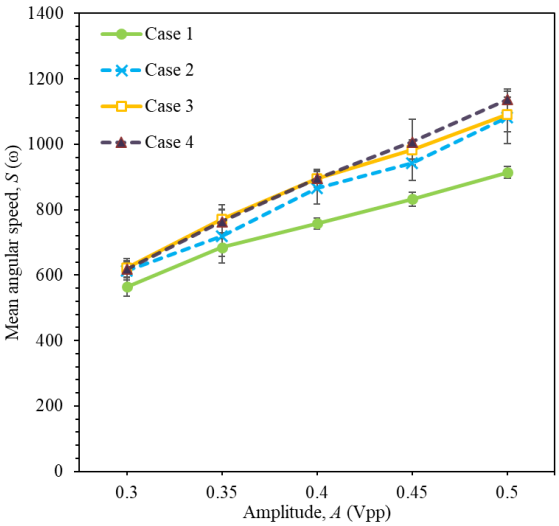

Fig. 10. Mean angular speed versus amplitude at constant frequency for different cases

Other than that, the graph reveals a diminishing difference between the mean angular speeds obtained for various cases. The most significant gap exists between Case 1 and Case 2, while the smallest disparity is evident between Case 3 and Case 4. This decreasing gap in mean angular speed suggests a tendency toward converging performance as the end cover diameters vary. The substantial difference in performance between Case 1 and Case 2 indicates that smaller end cover diameters tend to exhibit more pronounced variations in angular speed generation. As the end cover diameter increases from Case 2 to Case 4, the trend implies a diminishing impact of diameter variation on angular speed output. This observation may be attributed to the fact that, at a 93 mm diameter equivalent to the diameter of the resonator, the system attains a state of relative equilibrium where further increases in hole diameter do not significantly influence performance.

4.2 Introduction of Elliptic Nose Cone

The use of cone was reported to assist the bi-directional flow of thermoacoustics so that better performance can be achieved when the flow is guided properly into the rotor of the turbine [9]. This section focuses on the implementation of an elliptic nose cone within the bi-directional turbine, aiming to determine its impact on the overall performance of the system. The frequency modulation will range from 65 Hz to 120 Hz, incrementing at 5 Hz intervals to identify the resonance frequency. Measurement parameters encompass voltage, angular speed, and pressure differentials before and after the turbine. Subsequently, the collected experimental data will be calculated to determine the power output of the bi-directional turbine. A comparative analysis will then be conducted, evaluating the power generation between scenarios with and without the elliptic nose cone. Figure 11 shows the impact of introducing the elliptic nose cone into the system in relation to the angular speed as the frequency varies from 65 Hz to 120 Hz.

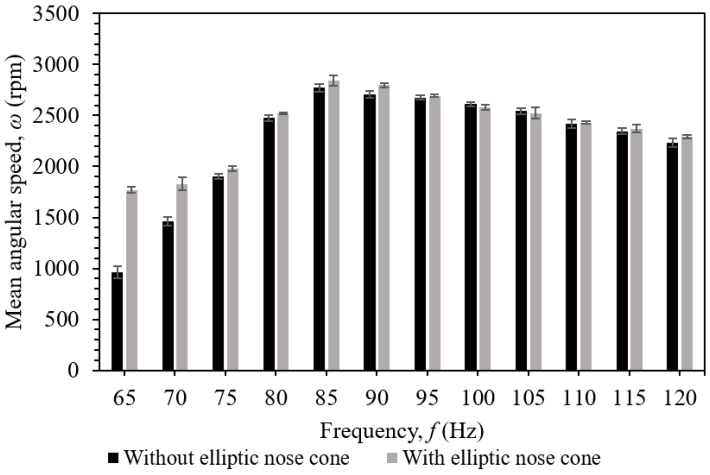

Fig. 11. Mean angular speed versus frequency with and without elliptic nose cone

The graph highlights a marginal increase in angular speed with the presence of the elliptic nose cone compared to its absence, especially for cases with frequency higher than 75 Hz. This observed enhancement can be attributed to the guiding effect imparted by the elliptic nose cone, facilitating improved flow dynamics within the system. From previous studies, it is found that the best nose cone for a thermoacoustic system is of an elliptical shape among hemispherical and parabolic shapes [9]. The rationale behind this superiority lies in the aerodynamic characteristics of an elliptical shape, which, when applied as a nose cone, facilitates smoother and more efficient flow dynamics. The elliptical shape is known to minimize drag and streamline the flow, creating a conducive environment for the thermoacoustic system [27]. At flow frequency lower than the 75 Hz, the presence of elliptic nose is very helpful in making the turbine flow faster and consequently generating more power.

In the context of the current study, the positive impact on angular speed can be understood as a result of the elliptic nose cone optimizing the flow patterns, reducing turbulence, and effectively guiding the working medium. This corroborates the notion that the significance of specific shape of the nose cone in influencing the performance of thermoacoustic systems. Therefore, the marginal increase in angular speed observed in the presence of the elliptic nose cone aligns with the aerodynamic benefits associated with this shape, as supported by the previous studies [9].

Furthermore, an insightful observation derived from the graph is the identification of the resonance frequency for both cases. The angular speed for both configurations attain its maximum value at 85 Hz and exhibits a gradual decline thereafter. This trend serves as evidence affirming that the resonance frequency of the system occurs precisely at 85 Hz. Resonance frequency, in the context of thermoacoustic systems, represents the frequency at which the system's natural oscillations are most effectively amplified. The peak angular speed at the resonance frequency indicates optimal energy transfer and efficient conversion within the system. The resonance frequency is important in ensuring the efficient transfer of acoustic power to the electricity-generating component within thermoacoustic system [9].

Drawing a parallel to the current experiment, the observed peak in angular speed at 85 Hz, identified as the resonance frequency, substantiates previous findings [9]. The alignment of the system's natural oscillations with the working frequency corresponds to the optimal conditions for power generation. Therefore, the resonance frequency is important for maximizing the effectiveness of thermoacoustic systems in converting acoustic power to electrical energy. Apart from that, the pressure before and after the bi-directional turbine with installation of elliptic nose cone is as shown in the Figure 12.

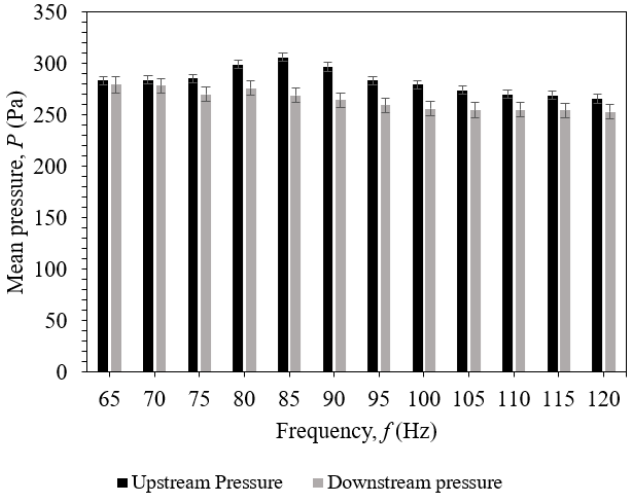

Fig. 12. Pressure variations before and after the bi-directional turbine with the installation of the elliptic nose cone

The observed pressure drops before and after the bi-directional turbine are intricately linked to the fundamental principles of thermoacoustic systems. The conversion of acoustic energy into rotational motion, as manifested by the pressure drops, aligns with the cyclic compression and expansion of the working medium within the system, guided by acoustic waves [28]. In the context of a thermoacoustic system, the pressure drops across the bi-directional turbine is a testament to the effectiveness of the system in translating acoustic energy into mechanical work. As the working medium undergoes compression before entering the turbine, a high-pressure region is established. The subsequent expansion of the working medium as it passes through the turbine induces the rotation of the turbine blades, converting the pressure-induced mechanical work into electricity or other useful outputs.

After knowing the pressure variations before and after the bi-directional turbine, the mean pressure drop with the increase of frequency can be determined, as illustrated in Figure 13. From the graph, the greatest pressure drop is found to be at the resonance frequency which is 85 Hz. Thermoacoustic system experiences a synchronized and maximized response to the acoustic waves generated at its resonance frequency [28]. This synchronization leads to a more efficient conversion of acoustic energy into mechanical work in the bi-directional turbine. Also at the resonance frequency, the amplitude of acoustic waves is maximized. This means that the cyclic compression and expansion of the working medium reach their peak, creating more significant pressure fluctuations. Besides, the resonance frequency corresponds to the natural frequency of the system, where the mechanical and acoustic components are in harmony [29]. This alignment facilitates optimal energy transfer between the acoustic waves and the bi-directional turbine. Also, the pressure drops across the turbine is directly related to the conversion of acoustic energy into rotational motion. At resonance frequency, the efficiency of this conversion process is maximized, leading to the largest pressure drop across the turbine.

Apart from that, the observation of relatively small pressure drops in both scenarios, with and without the elliptic nose cone, is consistent with the characteristics of loudspeakers as described by other studies [19]. Loudspeakers, being generally situated in a low impedance region, experience smaller pressure drops. This aligns well with the experiment's data, where the pressure drops across the bi-directional turbine are indeed modest, ranging from 3.10 Pa to 36.89 Pa. The contextualization of this observation within the framework provided by the work of previous study reinforces the

understanding that loudspeakers, despite their limitations in high-power and high-acoustic amplitude scenarios, remain functional when the pressure difference across the cone is within the kPa range [19].

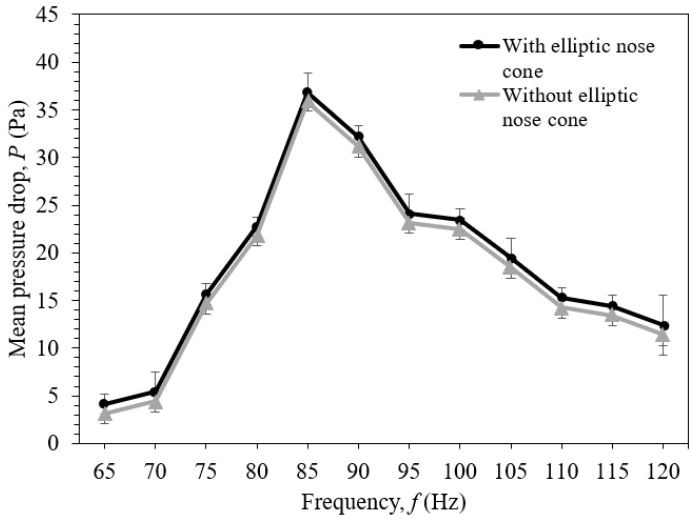

Fig. 13. Mean pressure drop across bi-directional turbine with the increase of frequency

The marginal difference in pressure drops between the scenarios with and without the elliptic nose cone, where the scenario without the nose cone exhibits a slightly lower pressure drop (approximately 1 Pa less), can be attributed to the constraints imposed by the insufficient length of the resonator. The resonator's limited length poses a challenge to the effective guidance of the flow by the elliptic nose cone, especially since the nose cone surpasses the length of the resonator. This limitation hinders the optimal functioning of the nose cone in directing the flow, leading to a situation where the guiding effect is significantly compromised. After the power generated by the bi-directional turbine is calculated, the comparison of power generated by the rotor with and without the presence of elliptic nose is plotted and shown in Figure 14.

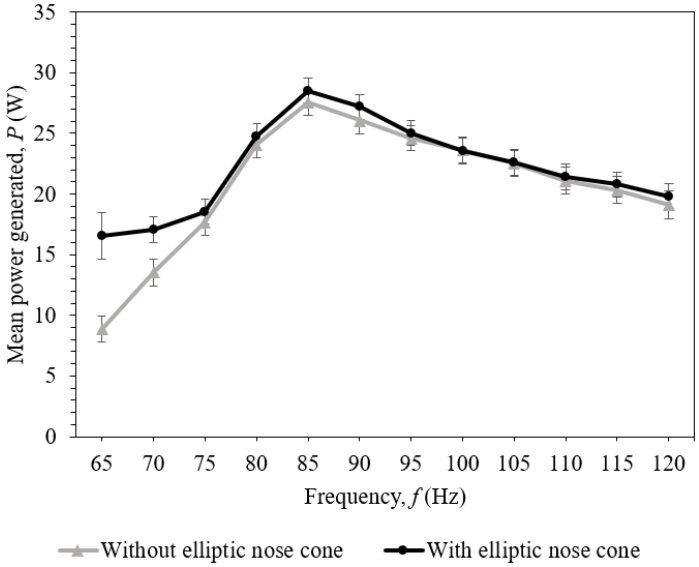

Fig. 14. Comparison of mean power generated by bi-directional turbine with and without elliptic nose cone

The graph illustrates a nuanced increase in the power generated by the bi-directional turbine when equipped with the elliptic nose cone as opposed to its counterpart without the nose cone. Notably, the peak power output is achieved at 85 Hz, totalling 28.5 W, compared to the configuration lacking the elliptic nose cone, which produced 27.55 W. This observed enhancement in power generation aligns with the guiding principle that the elliptic nose cone contributes to improved flow dynamics within the system. The systematic guidance of airflow facilitated by the elliptic nose cone enhances the interaction between the working medium and the turbine blades, optimizing the conversion of acoustic energy into mechanical work [9].

According to Figure 14, there is a substantial discrepancy in mean power generated between the scenarios with and without the elliptic nose cone at 65 Hz, amounting to 16.5 V and 8.87 V, respectively. In contrast, variations in power between the two scenarios at other frequencies are relatively smaller, ranging around 1 to 2 volts. This discrepancy in mean power generated between the scenarios with and without the elliptic nose cone at 65 Hz can be attributed to the resonant behaviour and the guiding effect of the elliptic nose cone. At resonant frequencies, the interaction between the acoustic waves and the bi-directional turbine is maximized, leading to an enhanced power output. The resonant frequency of the system, as identified at 85 Hz in this study, represents a condition where the turbine responds most effectively to the acoustic waves. At 65 Hz, which is below the resonant frequency, the guiding effect of the elliptic nose cone becomes more pronounced. The cone is designed to streamline and enhance the flow dynamics, guiding the acoustic waves more effectively towards the bi-directional turbine. This improved guidance results in a more efficient interaction between the acoustic waves and the turbine, leading to a substantially higher mean power output compared to scenarios without the nose cone. As the frequency deviates further from the resonant frequency, the impact of the nose cone diminishes, and the differences in mean power between the scenarios become less significant. The resonant frequency acts as a critical point where the combined effects of the guiding nose cone and the inherent system resonance result in optimal energy transfer to the bi-directional turbine.

5. Conclusion

The varying of variables, ranging from end cover diameters to the introduction of an elliptic nose cone has provided some understanding into optimizing system performance. Varying hole diameters demonstrated a direct correlation with system parameters. The 93 mm diameter of hole exhibited the highest voltage and angular speed, emphasizing the significance of system openness. The introduction of an elliptic nose cone showcased a marginal increase in angular speed, affirming its role in enhancing flow dynamics. Additionally, the system's resonance frequency was identified at 85 Hz, indicating the importance of tailoring components to optimal operating frequencies.

Acknowledgement

The authors would like to thank Universiti Teknikal Malaysia Melaka for funding the publication and providing the research facilities for the investigation.

References

[1] Swift, G. W., and Steven L. Garrett. "Thermoacoustics: A Unifying Perspective for Some Engines and Refrigerators." *The Journal of the Acoustical Society of America* 113, no. 5 (2003): 2379-2381. https://doi.org/10.1121/1.1561492

[2] Chen, Geng, Lihua Tang, Brian Mace, and Zhibin Yu. "Multi-physics coupling in thermoacoustic devices: A review." *Renewable and Sustainable Energy Reviews* 146 (2021): 111170. https://doi.org/10.1016/j.rser.2021.111170

[3] Alamir, Mahmoud A. "Thermoacoustic energy conversion devices: novel insights." *Journal of Advanced Research in Fluid Mechanics and Thermal Sciences* 77, no. 2 (2021): 130-144. https://doi.org/10.37934/arfmts.77.2.130144
[4] Liu, Dongdong, Yanyan Chen, Wei Dai, and Ercang Luo. "Acoustic characteristics of bi-directional turbines for thermoacoustic generators." *Frontiers in Energy* 16, no. 6 (2022): 1027-1036. https://doi.org/10.1007/s11708-020-0702-3
[5] Alcock, A. C., L. K. Tartibu, and T. C. Jen. "Experimental investigation of an adjustable thermoacoustically-driven thermoacoustic refrigerator." *International Journal of Refrigeration* 94 (2018): 71-86. https://doi.org/10.1016/j.ijrefrig.2018.07.015
[6] Bhatti, Umar Nawaz, Salem Bashmal, Sikandar Khan, and Rached Ben-Mansour. "Numerical modeling of standing wave thermoacoustic devices–A review: Modélisation numérique des dispositifs thermoacoustiques à ondes stationnaires–Une revue." *International Journal of Refrigeration* 146 (2023): 47-62. https://doi.org/10.1016/j.ijrefrig.2022.09.024
[7] Yang, Zongming, Volodymyr Korobko, Mykola Radchenko, and Roman Radchenko. "Improving thermoacoustic low-temperature heat recovery systems." *Sustainability* 14, no. 19 (2022): 12306. https://doi.org/10.3390/su141912306
[8] Biwa, Tetsushi. *Introduction to thermoacoustic devices*. World Scientific Publishing Co. Pte Ltd, 2023.
[9] Timmer, Michael Andreas Gerardus. "Bidirectional impulse turbines for thermoacoustic devices." PhD thesis, University of Twente, 2020.
[10] Hasbullah, Nurjannah, Fatimah Al Zahrah Mohd Saat, Fadhilah Shikh Anuar, Dahlia Johari, and Mohamad Firdaus Sukri. "Temperature and Velocity Changes Across Tube Banks in One-directional and Bi-directional Flow Conditions." *Evergreen* 8, no. 2 (2021): 428-437. https://doi.org/10.5109/4480725
[11] Sugiyanto, Sugiyanto, Samsul Kamal, Joko Waluyo, and Adhika Widyaparaga. "The Experiment Study on the Utilization of Standing Wave Thermoacoustic Engine to Drive Wells Bi-Directional Turbine." In *Journal of Physics: Conference Series*, vol. 1772, no. 1, p. 012026. IOP Publishing, 2021. https://doi.org/10.1088/1742-6596/1772/1/012026
[12] Liu, Dongdong, Yanyan Chen, Wei Dai, and Ercang Luo. "Numerical Analysis of Bi-directional Impulse Turbine Performance for Thermoacoustic Power Generators." *Energy Procedia* 158 (2019): 1986-1992. https://doi.org/10.1016/j.egypro.2019.01.457
[13] De Blok, Kees, Pawel Owczarek, and Maurice-Xavier Francois. "Bi-directional turbines for converting acoustic wave power into electricity." In *9th PAMIR International Conference, Riga, Latvia.* 2014.
[14] Saad, Mina, Manuel García Díaz, Bruno Pereiras, and José González. "Optimized geometry design of a radial impulse turbine for OWC wave energy converters." *Applied Ocean Research* 111 (2021): 102650. https://doi.org/10.1016/j.apor.2021.102650
[15] Radulescu, Dan, Georgel Vizitiu, and Marius Deaconu. "Numerical study of a thermoacoustic impulse turbine." In *AIP Conference Proceedings*, vol. 2116, no. 1. AIP Publishing, 2019. https://doi.org/10.1063/1.5114369
[16] Liu, Liu, Peng Yang, and Yingwen Liu. "Comprehensive performance improvement of standing wave thermoacoustic engine with converging stack: Thermodynamic analysis and optimization." *Applied Thermal Engineering* 160 (2019): 114096. https://doi.org/10.1016/j.applthermaleng.2019.114096
[17] Timmer, Michael A. G., and Theo H. Van Der Meer. "Characterization of bidirectional impulse turbines for thermoacoustic engines." *The Journal of the Acoustical Society of America* 146, no. 5 (2019): 3524-3535. https://doi.org/10.1121/1.5134450
[18] Elatife, Khalid, and Abdellatif El Marjani. "Optimization design procedure of a radial impulse turbine in OWC system." *International Energy Journal* 18, no. 4 (2018).
[19] Timmer, Michael A. G., Kees de Blok, and Theo H. van der Meer. "Review on the conversion of thermoacoustic power into electricity." *The Journal of the Acoustical Society of America* 143, no. 2 (2018): 841-857. https://doi.org/10.1121/1.5023395
[20] Fleming, Conor F., and Richard H. J. Willden. "Analysis of bi-directional ducted tidal turbine performance." *International Journal of Marine Energy* 16 (2016): 162-173. https://doi.org/10.1016/j.ijome.2016.07.003
[21] Zhang, Zhiguo, Dan Zhao, R. Dobriyal, Youqu Zheng, and Wenming Yang. "Theoretical and experimental investigation of thermoacoustics transfer function." *Applied Energy* 154 (2015): 131-142. https://doi.org/10.1016/j.apenergy.2015.04.026
[22] Ali, Ussama, Omar Al-Mufti, and Isam Janajreh. "Harnessing sound waves for sustainable energy: advancements and challenges in thermoacoustic technology." *Energy Nexus* (2024): 100320. https://doi.org/10.1016/j.nexus.2024.100320
[23] Sujith, R. I., and Samadhan A. Pawar. *Thermoacoustic Instability*. Berlin/Heidelberg, Germany: Springer International Publishing, 2021.

[24] Saat, Fatimah Al Zahrah Mohd, Nurhafizah Nordin, Nur Damia Asma Rosle, and Safarudin Ghazali Herawan. "A 3D Printed bi-directional Turbine for Thermoacoustic Standing Wave Environment at an Atmospheric Pressure." *Journal of Advanced Research in Experimental Fluid Mechanics and Heat Transfer* 15, no. 1 (2024): 1-13. https://doi.org/10.37934/arefmht.15.1.113

[25] Elhawary, M. A., Abdelmaged H. Ibrahim, Ashraf S. Sabry, and Ehab Abdel-Rahman. "Experimental study of a small scale bi-directional axial impulse turbine for acoustic-to-mechanical power conversion." *Renewable Energy* 159 (2020): 414-426. https://doi.org/10.1016/j.renene.2020.05.162

[26] Dunn, F., W. M. Hartmann, D. M. Campbell, and Neville H. Fletcher. *Springer handbook of acoustics*. Springer, 2015.

[27] Prajapati, Sheetal, Ankit Kumar Mishra, and Masetty Akshay. "Comparative Study on Nose Cones with respect to Angle of Attack using CFD." *REST Journal on Advances in Mechanical Engineering* 1, no. 4 (2022): 7-12. https://doi.org/10.46632/jame/1/4/2

[28] Daschewski, Maxim, Rainer Boehm, Jens Prager, Marc Kreutzbruck, and Andrea Harrer. "Physics of thermo-acoustic sound generation." *Journal of Applied Physics* 114, no. 11 (2013). https://doi.org/10.1063/1.4821121

[29] Garrett, Steven L. *Understanding acoustics: an experimentalist's view of sound and vibration*. Springer Nature, 2020. https://doi.org/10.1007/978-3-030-44787-8